SPANDIDOS PUBLICATIONS

ONCOLOGY REPORTS 45: 1306-1314, 2021

Repurposing of a monoamine oxidase A inhibitor-heptamethine carbocyanine dye conjugate for paclitaxel-resistant non-small cell lung cancer

XIAO-GUANG YANG[1*], YAN-YU LI[1*], DONG-XUE ZHAO[1], WEI CUI[2], HAN LI[2], XIN-YU LI[2], YU-XIN LI[2] and DUN WANG[1]

[1]School of Pharmaceutical Engineering and [2]Department of Pharmacology, Shenyang Pharmaceutical University, Shenyang, Liaoning 110016, P.R. China

Received March 10, 2020; Accepted October 15, 2020

DOI: 10.3892/or.2021.7950

Abstract. Non-small cell lung cancer (NSCLC) remains an intractable disease, which is primarily due to tumor metastasis and the acquisition of resistance to chemotherapy. Therefore, there is an urgent need for novel therapeutics to overcome these obstacles. It was recently demonstrated that upregulated expression of monoamine oxidase A (MAOA) contributes to the progression of NSCLC. G10, a tumor-targeting representative conjugate of heptamethine carbocyanine dye and an inhibitor of MAOA, was shown to exert potent cytotoxic effects, comparable to those of doxorubicin, against prostate cancer cell lines, as well as moderate MAOA inhibitory activity. The research described herein aimed to extend our previous study on the antitumor function of G10 in NSCLC *in vitro* and *in vivo*, and to elucidate the mechanisms through which G10 exerts its antineoplastic effects. G10 markedly inhibited the proliferation of paclitaxel-resistant NSCLC cells (H460/PTX) and reduced tumor cell migration and invasion. Gene expression profiling of paclitaxel-resistant NSCLC cells following treatment with G10 demonstrated that the expression of genes associated with the extracellular matrix was significantly affected, particularly the metastasis-related genes matrix metallopeptidase (MMP)2, MMP14 and COL6A, which exhibited notably reduced expression. Additionally, the results also demonstrated that MAOA-related pathways, including AKT and hypoxia-inducible factor-1α, were also inhibited by G10 treatment and, subsequently, the downstream molecules of these pathways, such as p21, MMP2 and vascular endothelial growth factor, were also downregulated, highlighting a possible mechanism through which G10 suppresses tumor cell migration, invasion and proliferation. Importantly, in mouse NSCLC xenografts, combined treatment with G10 and paclitaxel resulted in pronounced inhibition of tumor growth. Taken together, the results of the present study highlight the potential of G10 as a novel therapeutic targeting MAOA in paclitaxel-resistant NSCLC.

Introduction

Non-small cell lung cancer (NSCLC), including adenocarcinoma, squamous cell carcinoma and large-cell carcinoma, is the most common subtype of lung cancer (1,2). Currently, the standard treatment options for patients with advanced NSCLC include chemotherapy, targeted therapy and immunotherapy, with traditional chemotherapeutics such as cisplatin and paclitaxel (PTX), epidermal growth factor receptor tyrosine kinase inhibitors (TKIs) and immune checkpoint inhibitors (3). However, tumor metastasis and drug resistance limit the efficacy of these drugs (4). Thus, considerable efforts are focused on identifying new targets and developing novel therapeutic methods.

Mitochondrial outer membrane-anchored monoamine oxidase (MAO) catalyzes the oxidative deamination of various monoamines, including dopamine, 5-hydroxytryptamine, norepinephrine, phenethylamine and tyrosine (5). MAOA, a subtype of MAO, is mainly distributed in catecholaminergic neurons (6). MAOA inhibitors are primarily used for treatment of nervous disorders, depression and anxiety (7). However, it was recently demonstrated that overexpression of MAOA contributed to prostate cancer (PCa) progression and the degree of malignancy (8,9). Multiple studies have investigated the mechanism through which MAOA promotes PCa progression and demonstrated that MAOA functionally induces epithelial-to-mesenchymal transition (EMT) through activation of a vascular endothelial growth factor (VEGF)A/neuropilin-1 signaling pathway and the protein kinase B (AKT)/FOXO1 pathway, stabilizing hypoxia-inducible factor-1α (HIF-1α) by generating reactive oxygen species (9).

Overexpression of MAOA was also observed in Hodgkin lymphoma and brain glioma (10). Furthermore, MAOA

Correspondence to: Professor Dun Wang, School of Pharmaceutical Engineering, Shenyang Pharmaceutical University, 103 Wenhua Road, Shenyang, Liaoning 110016, P.R. China
E-mail: wangduncn@hotmail.com

*Contributed equally

Key words: non-small cell lung cancer, monoamine oxidase A, heptamethine carbocyanine dye, antitumor

inhibitors have shown promising inhibitory effects on several types of tumors, such as PCa, classical Hodgkin lymphoma and resistant gliomas (11-13). The role of MAOA in NSCLC has also been reported, with MAOA expression found to be significantly increased in cancerous tissue, and possibly associated with the expression of EMT-promoting genes (N-cadherin, Slug and TWIST) (14). These results indicate that MAOA may play a pivotal role in promoting the progression of NSCLC by mediating EMT. Thus, MAOA inhibitors may hold considerable promise as treatment for NSCLC.

Near-infrared heptamethine carbocyanine dyes have been used for optical therapy and imaging due to their excellent fluorescence properties, and can generate fluorescence emissions in the range of 700-1,000 nm (15,16). Of particular relevance is that some heptamethine carbocyanine dyes preferentially accumulate in tumor tissues (17-19). The selective accumulation of these dyes in neoplastic rather than normal tissues is induced by organic anion transporting polypeptides (OATPs), a hypoxic tumor environment and an increased mitochondrial membrane potential in cancer cells (20-22). Therefore, heptamethine carbocyanine dyes may serve as functional selective transporters of therapeutic drugs to tumors. In our previous study, the non-selective small molecule MAOA inhibitor isoniazid was used to target MAOA, and was coupled with heptamethine carbocyanine dyes via amide bonds to design and synthesize tumor-targeting MAOA inhibitor-heptamethine carbocyanine dye conjugates (23). Amongst these conjugates, compound G10 demonstrated potent cytotoxicity against PC-3 cells. The MAOA inhibitory activity of G10 was consistent with the cell viability assay results. The aim of the present study was to investigate the effects of G10 against NSCLC *in vitro* and *in vivo* and elucidate the underlying antitumor molecular mechanisms.

Materials and methods

Materials. 4-Methylphenylhydrazine hydrochloride, 4-methoxyphenylhydrazine hydrochloride and other chemical intermediates were purchased from Meryer Chemical Technology Co., Ltd.; 3-methyl-2-butanone and isoniazid were purchased from Aladdin Reagent Company. Other reagents were all synthesized in the laboratory. Primary antibodies against hypoxia-inducible factor-1α (HIF-1α, cat. no. 3716, dilution 1:1,000), matrix metallopeptidase 2 (MMP2, cat. no. 87809, dilution 1:1,000), vascular endothelial growth factor (VEGF, cat. no. 2463, dilution 1:1,000), phosphorylated AKT (p-AKT, cat. no. 4060, dilution 1:2,000), AKT (cat. no. 9272, dilution 1:1,000), p21 (cat. no. 2947, dilution 1:1,000) and β-actin (cat. no. 4970, dilution 1:2,000), were obtained from Cell Signaling Technology, Inc.

Synthesis of G10. 2,3,3,5-Tetramethyl-3*H*-indole (intermediate compound 1A; 5 g; 28.9 mmol) and ethyl 4-bromobutyrate (28 g; 144 mmol) were added to 200 ml CH_3CN and the reaction proceeded under reflux for 40 h. After purification with silica column chromatography, 4 g of a yellow oily liquid was obtained. Subsequently, the obtained intermediate was dissolved in 20 ml 5 mol/l HCl and heated to reflux for 14 h to obtain 3 g of a colorless liquid (intermediate compound 2A), with a yield of 81%. 5-Methoxy-2,3,3-trimethyl-3*H*-indole (5 g; 26.5 mmol) and 1-bromobutane (17.9 g; 132 mmol) were suspended in 200 ml CH_3CN, and the mixture was refluxed for 40 h. Colorless liquid (intermediate compound 2B; 3.5 g; yield, 41%) was obtained by purification with a silica gel column. Next, 1-phenylamino-5-phenylimino-1,3-pentadiene hydrochloride (1 g; 3.5 mmol), 2B (1.14 g; 3.5 mmol) together with 1 ml Et_3N were added to 30 ml acetic anhydride at 50˚C for 1 h. After cooling to an ambient temperature, the reaction mixture was poured into 500 ml Et_2O and filtered to obtain 1.5 g of a brownish precipitate (intermediate compound 3; yield, 83%). Subsequently, intermediate 3 (1 g; 1.92 mmol) and intermediate 2A (649 mg; 1.92 mmol) were added to 30 ml pyridine and heated to 50˚C with stirring for 1 h. The mixture was evaporated under reduced pressure and acidified to obtain intermediate compound 4 (300 mg; yield, 24%) that was purified with a silica gel column. Finally, PyBOP (241 mg; 0.46 mmol), N,N-diisopropylethylamine (DIPEA; 59 mg; 0.46 mmol) and intermediate 4 (300 mg; 0.46 mmol) were added to 100 ml dichloromethane of ice-salt bath, and isoniazid (63 mg; 0.46 mmol) was added. The resulting mixture was stirred for an additional 24 h at room temperature, filtered, and the solvent was removed by reduced pressure distillation and purified by silica gel to obtain G10 (90 mg; yield, 26%).

Cell lines and culture. A549, NCI-H460 and PC9 human lung adenocarcinoma cell lines were purchased from American Type Culture Collection. Cells were cultured in RPMI-1640 medium supplemented with 10% FBS (both from Gibco; Thermo Fisher Scientific, Inc.), and maintained at 37˚C in a humidified incubator with 5% CO_2. The chemoresistant cells were obtained after treatment with cisplatin, PTX and erlotinib (MedChemExpress) at concentrations between 0.5 and 5 μM for 3 months.

MAOA enzymatic activity assay. MAOA enzymatic activity was measured in A549, A549/CDDP, A549/PTX, H460, H460/CDDP, H460/PTX, PC9 and PC9/Er cells as described previously (24). Briefly, cells were plated in culture medium supplemented with 10% FBS in a 10-mm dish for 24 h. Through extracting the reaction products, MAOA activity was measured using a Cell MAOA assay kit (Shanghai Chengong Biotechnology) according to the manufacturer's protocol, and was based on substrate p-tyramine levels following treatment with the MAOB inhibitor pargyline.

Cell viability assay. An MTT assay was used to determine the effects of G10 on cell viability *in vitro*. Briefly, cells ($1x10^5$ cells/ml) were seeded into 96-well culture plates and incubated overnight. Subsequently, the cells were treated with a range of concentrations (0.1-100 μM) of G10 for 72 h. MTT solution (10 μl, 2.5 mg/ml) was added to each well, and the plates were incubated for another 4 h at 37˚C. After centrifugation (1,000 x g for 10 min at room temperature), the medium was replaced with 100 μl DMSO. The optical density of these samples was measured using a Spectra Max Paradigm Reader (Molecular Devices, LLC) at 570 nm.

Flow cytometry analysis. Apoptosis analysis was performed using an Annexin V-FITC apoptosis detection kit (BioVision, Inc.). Cells ($1x10^6$) were treated with G10 for 48 h [RNA

interference cells were transfected with a specific MAOA siRNA or scramble siRNA (Santa Cruz Biotechnology, Inc.) for 24 h]. Subsequently, cells were collected by centrifugation (1,000 x g at 20˚C for 5 min) and resuspended in 500 μl binding buffer. Annexin V and PI were added to the cells. After incubation at room temperature for 5 mins in the dark, cells were analyzed using fluorescence activated cell sorting using a flow cytometer (Becton, Dickinson and Company). For autophagy analysis, the cells were treated with G10 for 48 h and incubated with MDC dye, followed by flow cytometry.

Microarray analysis and reverse transcription-quantitative PCR (RT-qPCR) analysis. Total RNA from untreated and G10-treated H460/PTX cells was isolated using an RNeasy Mini kit (Qiagen, Inc.) according to the manufacturer's protocol. Changes in gene expression were detected using an Affymetrix GeneChip PrimeView Human Gene Expression Arrays. In order to confirm the changes in specific gene expression, RT-qPCR was used. The sequences of the primers are listed in Table SI.

Transwell assays. Transwell chambers (Corning, Inc.) with 6.5-mm-diameter polycarbonate filters (pore size, 8 μm) were used to determine the effect of G10 on A549/PTX and H460/PTX cell migration and invasion *in vitro* (25). Briefly, the upper chambers of the insert were coated with Matrigel and the lower chambers were filled with fresh M200 medium (1% FBS) containing 10 ng/ml VEGF. After trypsinization, the cells were resuspended at a concentration of $1x10^6$ cells/ml in M200 containing 1% FBS and treated with different concentrations of G10 for 30 min at room temperature before seeding. A total of 100 μl of the cell suspension per well was loaded into the upper wells, and the chamber was incubated at 37˚C for 12 h. The cells were fixed and stained with Calcein-AM at room temperature for 30 min. Cells on the upper surface of the filter were removed by wiping with a cotton swab, and chemotaxis was quantified using the high-content drug screening system ImageXpressR Micro (Molecular Devices, LLC) by counting the cells that had migrated to the lower side of the filter.

Western blot analysis. A total of $1x10^7$ H460/PTX cells treated with G10 were collected. Western blotting was performed as previously described (26). Briefly, total proteins (50 μg) were extracted from the cells (determined by BCA method), resolved using 8-15% SDS-PAGE and transferred to PVDF membranes. The membranes were blocked with 5% non-fat dry milk at room temperature for three times (10 min/per times). Primary and secondary antibodies (Thermo Fisher Scientific, Inc.; cat. nos. 31430 and 31460, dilution 1:5,000) were then used to visualize the resolved proteins. Finally, an enhanced chemiluminescence system (ECL Plus; Amersham; Cytiva) was used to develop the blots.

In vivo antitumor efficacy studies. To evaluate the antitumor activity of G10 *in vivo*, a total of 20 7-8-week old male BALB/c nude mice (weight, 18-22 g) were anesthetized with 3% sodium pentobarbital (50 mg/kg, i.p.) and injected subcutaneously at the right flank with viable (confirmed using trypan blue staining) H460/PTX cells ($5x10^6$/100 μl PBS per mouse). When the mean subcutaneous size of the tumor reached 100 mm^3, the mice were randomly divided into four groups treated with different concentrations of G10 and a control group (4-6 mice per group). The G10 single treatment group and PTX single treatment group were administered G10 [19 mg/kg/2 days, intraperitoneally (i.p.); n=5] or PTX (3 mg/kg/2 days, i.p.; n=5), respectively. The combination group was treated with both G10 (19 mg/kg/2 days; i.p.; n=5) and PTX (3 mg/kg/2 days; i.p.; n=5). Tumor size was measured with a caliper every 3 days using the following formula: Tumor volume=shortest $diameter^2$ x longest diameter/2 (maximum tumor volume, 930 mm^3). Body weight was also recorded every 3 days. After 21 days, the mice were sacrificed with cervical dislocation, and lack of breathing and heartbeat for 3 min were observed to confirm death. The study protocol complied with the recommendations of the Guide for the Care and Use of Laboratory Animals of the Shenyang Pharmaceutical University and all animal experiments were approved by the Committee on the Ethics of Animal Experiments of the Shenyang Pharmaceutical University.

Statistical analysis. Differences between experimental groups were evaluated by one-way ANOVA followed by Turkey's post hoc test using the SPSS v.11.5 for Windows (SPSS, Inc.). $P<0.05$ (two-tailed test) was considered to indicate statistically significant differences.

Results

Chemical synthesis of G10. The target compound (G10) was synthesized as shown in Fig. 1 (23). First, intermediates 2A and 2B were synthesized by S_N2 nucleophilic substitution of 1A and 1B, with ethyl 4-bromobutyrate and 4-bromobutane as alkylating agents, respectively. Subsequently, the asymmetric heptamethine cyanine dye intermediate 4 was obtained by two-step aldol reactions of 2A and 2B reacting with 1-phenylamino-5-phenylimino-1,3-pentadiene hydrochloride in acetic anhydride, with pyridine as a catalyst. Finally, target compound G10 was obtained by condensation of compound 4 with isoniazid in the presence of DIPEA and PyBOP in anhydrous dichloromethane.

G10 significantly inhibits the proliferation and viability of PTX-resistant NSCLC cells exhibiting enhanced MAOA activity. In order to investigate the association between MAOA and drug resistance in lung cancer, the MAOA activity was examined in NSCLC cells resistant to chemotherapy (cisplatin and PTX), erlotinib-resistant NSCLC cells and their parental cells. As shown in Fig. 2A, the activity of MAOA was increased in chemotherapy-resistant NSCLC cells, but not in the TKI-resistant NSCLCs. In particular, PTX-resistant NSCLCs exhibited notably increased MAOA activity compared with the parental cells. Subsequently, cell viability was measured following treatment with the novel MAOA inhibitor G10. As shown in Fig. 2B, G10 exerted potent inhibitory effects on H460/PTX cells, and was more effective against the PTX-resistant cells compared with the parental cells (H460); in addition, the cytotoxicity of G10 was negatively correlated with MAOA activity, suggesting that inhibition of MAOA could reverse PTX resistance of NSCLC. To further confirm that G10 induced PTX-resistant cell death,

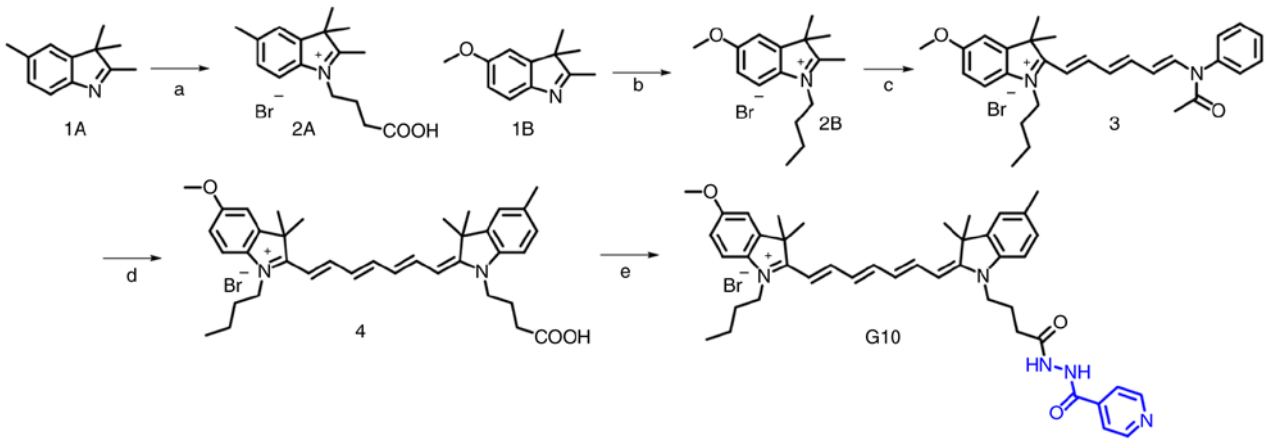

Figure 1. Synthesis of G10. (A) Ethyl 4-bromobutyrate, CH_3CN, 75˚C, 40 h; 5 mol/l HCl, 100˚C, 16 h; (B) 4-bromobutane, CH_3CN, 75˚C, 40 h; (C) 1-phenylamino-5-phenylimino-1,3-pentadiene hydrochloride, Et_3N, acetic anhydride, 50˚C, 1 h; (D) pyridine, 70˚C, 1 h; and (E) isoniazid, PyBOP, DIPEA, anhydrous DCM, room temperature.

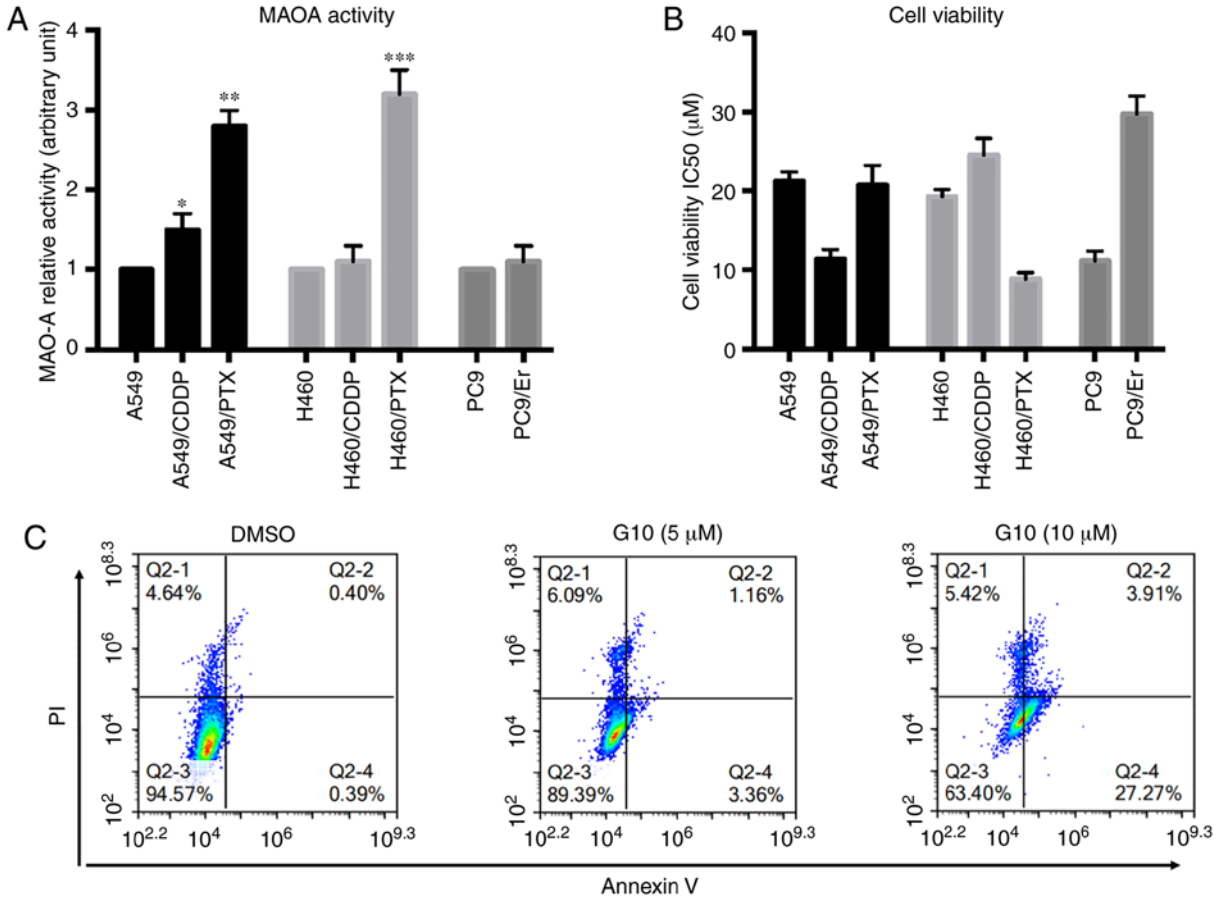

Figure 2. Relative MAOA activity and the ability of G10 to reduce cell viability in lung cancer cells lines. (A) Relative MAOA activity was determined using an MAOA enzymatic activity assay. (B) The effect of G10 (0.1, 1, 10 or 100 μM) on the viability of A549, A549/CDDP, A549/PTX, H460, H460/CDDP, H460/PTX, PC9 and PC9/Er cells was measured using an MTT assay. The IC_{50} values are shown. (C) Cell apoptosis was assessed by flow cytometry analysis in A549/PTX cells. Annexin V-positive cells were considered as apoptotic. $^{*}P<0.05$, $^{**}P<0.01$, $^{***}P<0.001$ vs. respective parental cell line. All experiments were repeated ≥2 times. MAOA, monoamine oxidase A; PTX, paclitaxel; CDDP, cisplatin; Er, erlotinib.

cell apoptosis was measured by flow cytometry (Fig. 2C). The results demonstrated that G10 induced cell apoptosis at relatively higher concentration (10 μM). Of note, when MAOA gene expression was knocked down, the apoptosis induced by G10 was abrogated (supplementary Fig. S1), indicating that cell apoptosis induced by G10 was dependent on MAOA activity.

G10 suppresses expression of extracellular matrix (ECM)-related genes. Acquisition of invasive ability by epithelial cells is required for metastasis (27). It has been previously demonstrated that MAOA promotes the proliferation, invasion and metastasis of PCa cells through inducing EMT and stabilizing HIF-1α (9). Therefore, the effect of G10 on the expression of

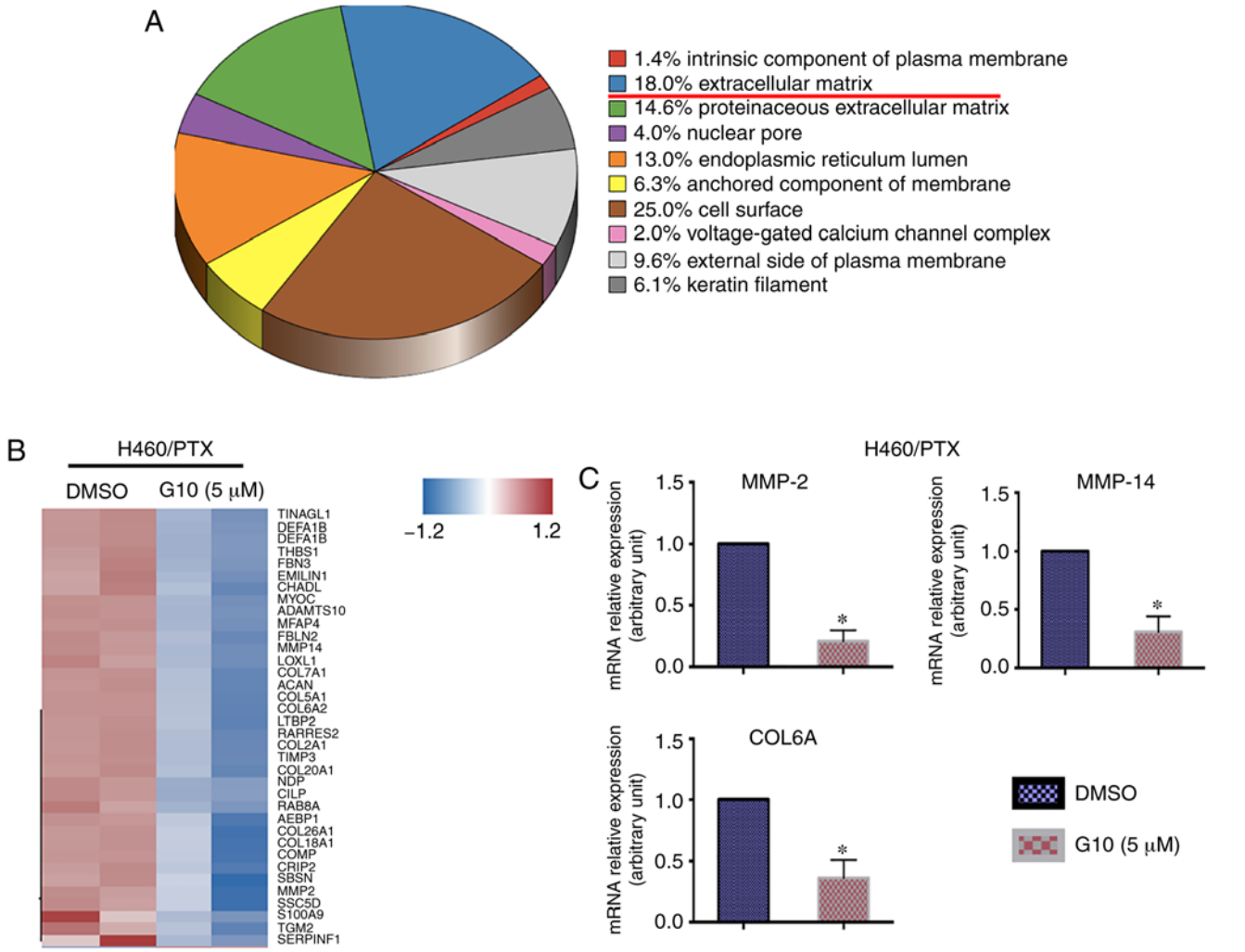

Figure 3. (A) Gene Ontology cellular component analysis of differentially expressed genes between G10-treated and -untreated H460/PTX cells. (B) Heatmap of differentially expressed extracellular matrix related genes. (C) MMP2, MMP14 and COL6A mRNA expression was measured in the H460/PTX cells treated with 5 μM G10 for 48 h under hypoxic conditions. MMP2, MMP14 and COL6A expression in the parental cells was used as the control. *P<0.05 compared with DMSO-treated cells. Data are presented as the mean ± the standard error of the mean, and all the experiments were repeated twice. PTX, paclitaxel; MMP, matrix metallopeptidase.

ECM-related genes, changes in which are closely associated with the migration, invasion and drug resistance of tumor cells, were examined. Using Gene Ontology (GO) cellular component (CC) analysis, the changes in the gene expression profile of H460/PTX cells, found to be relatively sensitive to G10 in the cell viability assay, following treatment with G10 were evaluated (Fig. 3A). The differentially expressed genes are involved in the intrinsic component of the plasma membrane, ECM, proteinaceous ECM, nuclear pores, endoplasmic reticulum lumen, anchored component of the membrane, cell surface, voltage-gated calcium channel complexes, external side of the plasma membrane and keratin filaments. Among these genes, the distinct changes in the expression of genes associated with the ECM that are closely associated with tumor cell migration, invasion and drug resistance were further explored (28-30). As shown in Fig. 3B, heatmap analysis was used to further analyze these genes, and revealed that changes in the expression levels of several genes associated with tumor invasion and migration. As MMP2, MMP14 and COL6A have been shown to be involved in the pathophysiological processes underlying migration and invasion of several types of cancer cells (31-33), the mRNA levels of MMP2, MMP14 and COL6A in H460/PTX cells following G10 administration was further explored. Treatment with G10 reduced the expression of MMP2, MMP14 and COL6A in H460/PTX cells (Fig. 3C). Of note, in addition to ECM-related genes, GO CC analysis suggested that the expression of cell surface-related genes was also significantly altered following treatment with G10. This may be explained by the fact that cell surface proteins may transduce signals from the ECM into the cells, which in turn regulate a range of cellular functions, such as survival, proliferation, migration and differentiation (34). Taken together, these results suggest that G10 may suppress tumor invasion and migration by affecting the expression of genes associated with the ECM.

G10 suppresses A549/PTX and H460/PTX cell migration and invasion in vitro. To determine whether G10 affects tumor cell migration and invasion, Transwell assays were performed. First, to avoid the direct cytotoxic effects of G10, Transwell assays were performed in cells treated with non-cytotoxic concentrations of G10 (cell viability >80%), which was determined using an MTT assay (data not shown). As shown in

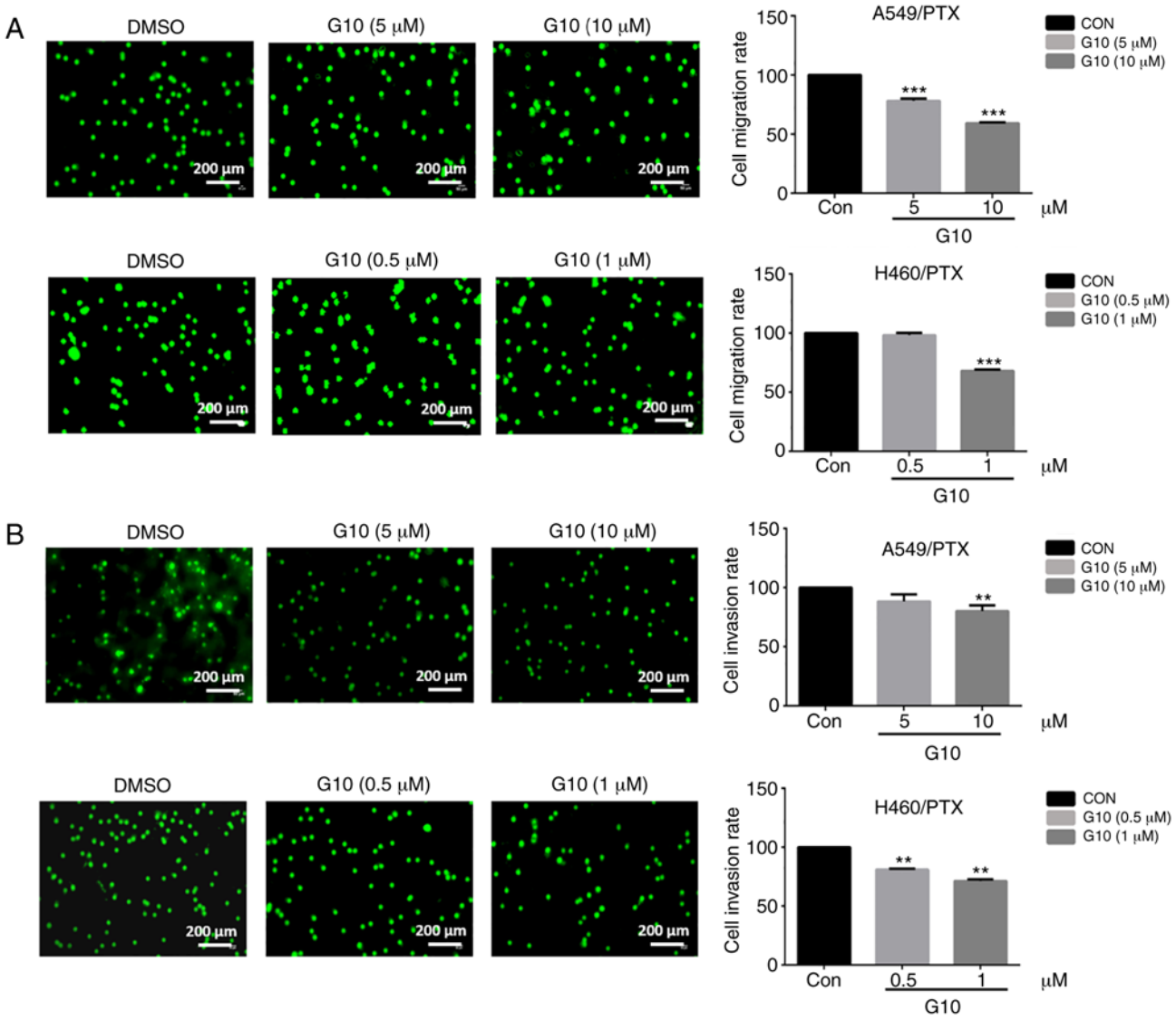

Figure 4. Effects of G10 on the migration and invasion of A549/PTX and H460/PTX cells. (A) A549/PTX and H460/PTX cell migration was assessed using Real-Time Cell Assessment following treatment with G10 (0, 5 or 10 μM and 0, 0.5 or 1 μM, respectively) for 24 h. Magnification, x200. (B) A549/PTX and H460/PTX cell invasion was assessed using Transwell assays following treatment with G10 for 12 h. Quantitative analysis of the effect of G10 on cell migration and invasion is presented as bar graph. Data are presented as the mean ± the standard error of the mean, and experiments were repeated three times. **P<0.01, ***P<0.001 vs. control. PTX, paclitaxel.

Fig. 4A, the number of migrating cells in both the A549/PTX and H460/PTX cell lines was decreased significantly following treatment with non-cytotoxic doses of G10. Similarly, G10 suppressed the invasive ability of A549/PTX and H460/PTX cells in a concentration-dependent manner (Fig. 4B). Taken together, these data suggest that G10 can inhibit the migration and invasion of PTX-resistant cells, consistent with the results of the GO CC analysis.

G10 reduces the expression of HIF-1α and the phosphorylation of AKT, increases the expression of p21 and induces autophagy. Upregulation of MAOA can activate HIF-1α and AKT signaling (9). The transcription factor HIF-1α mediates hypoxia by activating target genes associated with the mechanisms involved in tumor progression, such as increased tumor glycolysis, angiogenesis and metastasis (35). Activated HIF-1α regulates the expression of multiple genes in response to hypoxia, including VEGF (a key regulator of angiogenesis) and MMP2, which is an important enzyme promoting migration and invasion. Additionally, MMPs and VEGF are both involved in the metastatic process through modifying ECM components of neoplastic and stromal cells (36). HIF-1α, MMP2 and VEGF all participate in tumor invasion, migration and metastasis. The role of the MAOA-dependent HIF-1α/MMP2 and VEGF pathways on the inhibitory effects of G10 on cell invasion was examined using H460/PTX cells. As shown in Fig. 5A and B, G10 suppressed the expression levels of HIF-1α in a concentration-dependent manner and inhibited the expression of its target genes MMP2 and VEGF. Furthermore, the effects of G10 on the EMT biomarker E-cadherin were also assessed. The data revealed that G10 upregulated the expression of E-cadherin. These results suggest that G10 exerts its inhibitory effects on tumor cell migration and invasion through downregulating HIF-1α/MMP2 and VEGF under hypoxic conditions.

AKT, a serine/threonine kinase, requires phosphorylation to be activated to regulate cancer cell proliferation (37). G10

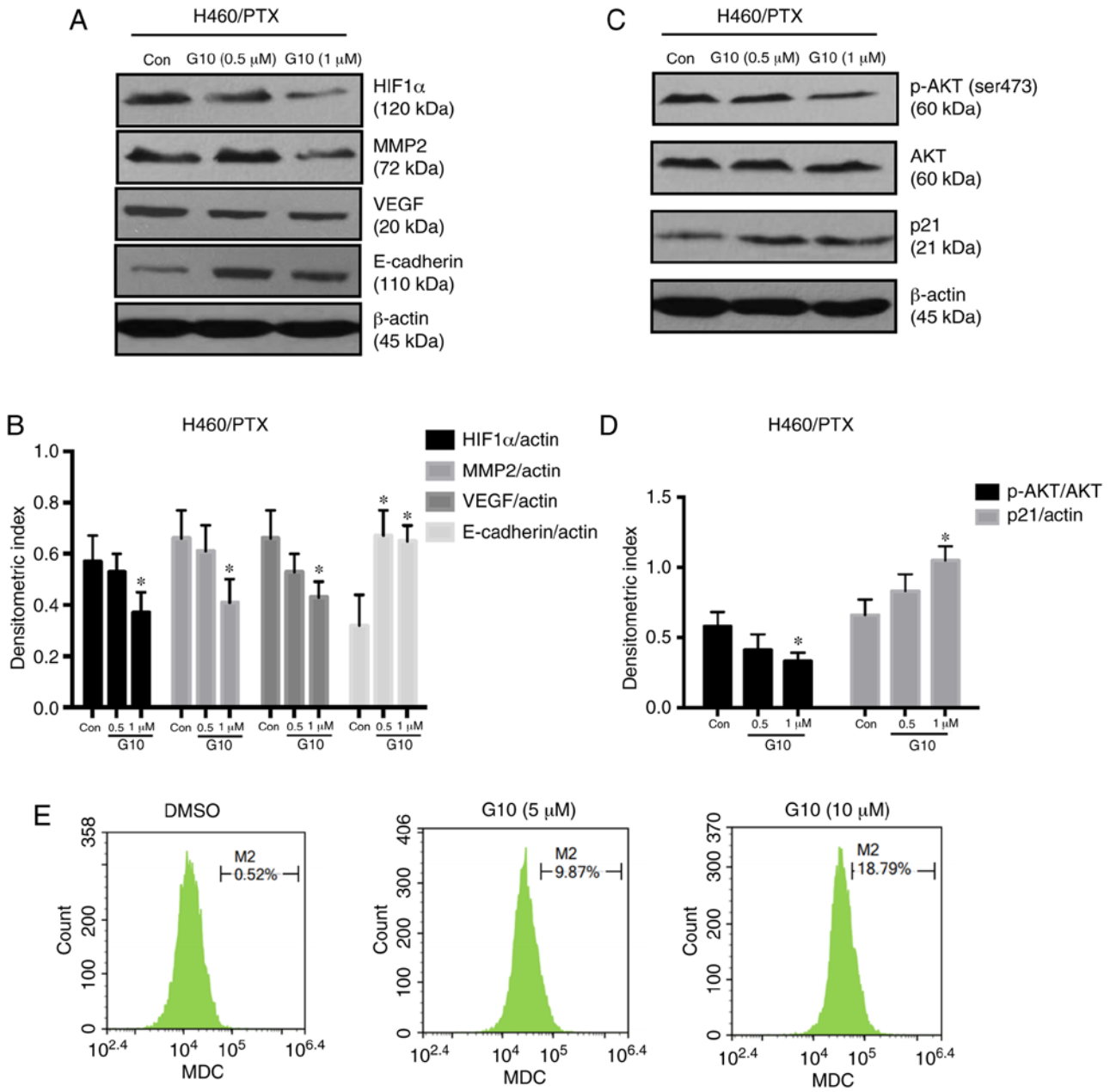

Figure 5. Effects of G10 on the expression levels of invasion-, migration- and proliferation-related proteins and on the autophagy of PTX-resistant cell lines. (A-D) Protein expression levels of HIF-1α, MMP2, VEGF, E-cadherin, p-AKT, AKT and p21 were assessed using western blot analyses of H460/PTX cells following treatment with G10 (0, 0.5 or 1 μM) for 48 h under hypoxic conditions. Densitometry analysis of western blot data was performed using the Quantity One system. β-actin expression was used as the loading control. (E) MDC content was measured by flow cytometry and was used to evaluate cell autophagy in A549/PTX cells. Data are presented as the mean ± the standard error of the mean, and experiments were repeated twice. *P<0.05 vs. control. PTX, paclitaxel; HIF, hypoxia-inducible factor; MMP, matrix metallopeptidase; VEGF, vascular endothelial growth factor; AKT, protein kinase B; MDC, monodansylcadaverine dye.

was shown to suppress AKT phosphorylation, thereby inhibiting AKT signaling (Fig. 5C and D). When AKT signaling is activated, the expression of p21, a tumor suppressor gene that is associated with tumor proliferation, is reduced. The results also confirmed that G10 treatment increased the expression of p21 (Fig. 5C and D), suggesting that inhibiting AKT signaling resulted in p21 activation. The mechanism underlying the suppressive effect of G10 on tumor progression may involve the regulation of the p-AKT/p21 signaling pathway. Due to the involvement of the AKT pathway in autophagy, cell autophagy was assessed using flow cytometry and was found to be induced by G10 in a concentration-dependent manner (Fig. 5E), suggesting that autophagy may also be involved in the antitumor effects of G10.

G10 combined with PTX reduces the growth rate of H460/PTX xenografts in vivo. As G10 exerted prominent antitumor effects *in vitro*, further investigation of the efficacy of G10 on the growth of H460/PTX xenograft models was assessed. In view of the obvious action of G10 on H460/PTX cells, they were selected to establish xenograft models. The results revealed that treatment with PTX exerted no significant effect on tumor growth (Fig. 6A), confirming that H460/PTX cells were PTX-resistant. In addition, treatment with G10 alone

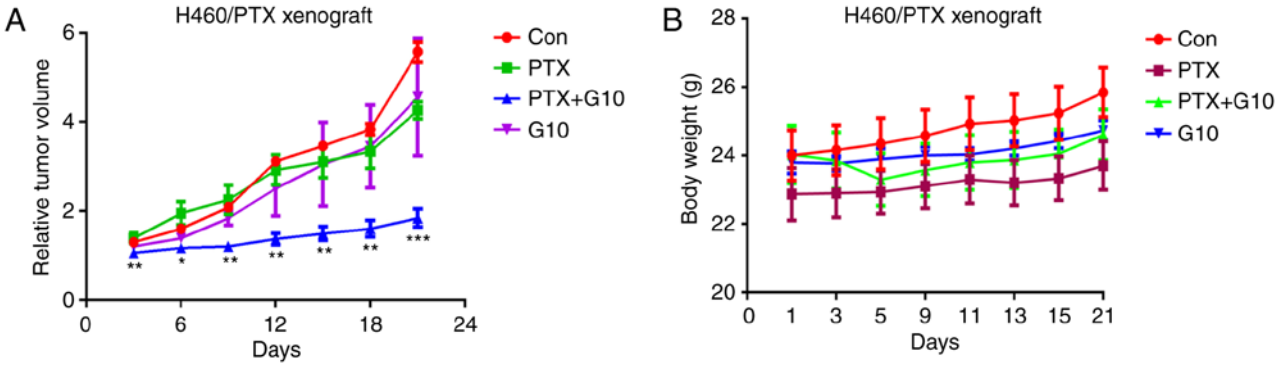

Figure 6. Effects of G10 on tumor growth of H460/PTX tumor xenografts in mice. Changes in (A) tumor volume and (B) mean body weight of the H460/PTX xenograft mice treated with G10 (19 mg/kg/2 days, i.p.) and PTX (3 mg/kg/2 days, i.p.) for 21 days. PTX, paclitaxel; Con, control; i.p. intraperitoneal. *P<0.05, **P<0.01, ***P<0.001 vs. control group.

was ineffective in inhibiting tumor progression. However, combined treatment with G10 and PTX significantly inhibited the growth of the H460/PTX xenografts within a 3-week treatment period (Fig. 6A). During this combined treatment, there were no notable differences in mouse body weight and visceral index (organ weight vs. body weight) between the control and treatment groups (Fig. 6B), suggesting that there were no gross toxic effects induced by the combination of G10 and PTX.

Discussion

Although MAOA appears to be a promising target for cancer therapy, the role of MAOA in NSCLC progression requires further elucidation. MAOA activity was assessed in a range of NSCLC cell lines, and PTX-resistant NSCLC cells were shown to exhibit increased MAOA activity. Therefore, the effects of G10, an isoniazide conjugate of a heptamethine dye targeting tumors and irreversible MAOA inhibitor, which was synthesized and described in our previous study, on NSCLC were assessed *in vitro* and *in vivo*. Despite being a notable structural transformation of isoniazide, the isoniazide moiety may still be the critical structure underlying the MAOA inhibitory activity of G10, based on our previous molecular docking analysis, showing that the larger cyanine dye could not enter into the active hydrophobic cavity of MAOA. More importantly, recent studies verified that cyanine dyes may serve as the vectors for targeting and delivering cargo to mitochondria in cancer cells (38,39). Nödling *et al* combined the mitochondria-targeting cyanine dyes Cy3 and Cy5 with ciprofloxacin (Cip) or the carboplatin derivative CPT, and evaluated the mitochondria-targeting ability and the cytotoxicity of the conjugates in human cervical carcinoma HeLa cells. The results revealed that the conjugates successfully accumulated in the mitochondria of HeLa cells and were more cytotoxic compared with their parent drug (increase in toxicity from 100-fold to 1,000-fold), indicating that the conjugation of drugs and cyanine dyes did not affect the uptake mechanism, but rather altered the subcellular localization of the conjugates (38). However, in the present study, the application of heptamethine dye greatly improved the antiproliferative activity of isoniazid against PTX-resistant NSCLC cells. This likely contributes to the mitochondria-targeting ability of heptamethine dyes and inhibition of the mitochondrial outer membrane enzyme MAOA. Choi *et al* also summarized the application of tumor-targeting heptamethine cyanine dyes in cancer treatment. These drug-dye conjugates were used in several cancers, such as brain cancer, Burkitt's lymphoma, prostate cancer and breast cancer (39). However, to the best of our knowledge, there has been no research on NSCLC treatment by heptamethine cyanine dye-drug conjugates to date. Hence, our findings may broaden the application of heptamethine dye-drug conjugates. Of note, the findings of the present study suggest that MAOA may be involved in the proliferation, migration and invasion of PTX-resistant NSCLC cells, and inhibition of MAOA may reverse PTX resistance of NSCLC. The conjugate G10 exerted a notable inhibitory effect on the migration and invasion of A549/PTX and H460/PTX cells. Additionally, G10 combined with PTX reduced the growth rate of H460/PTX xenografts, whereas treatment with G10 or PTX alone exerted no notable inhibitory effect. In conclusion, G10 may serve as an alternative treatment for PTX-resistant NSCLC. However, the mechanisms underlying the exact role of MAOA in PTX-resistant NSCLC require elucidation through further experimentation.

Acknowledgements

Not applicable.

Funding

No funding was received.

Availability of materials and data

The datasets used and/or analyzed during the present study are available from the corresponding author on reasonable request.

Authors' contributions

XGY contributed to the conception and design of the study, analyzed and interpreted the research data, and drafted the manuscript. YYL was a major contributor to writing the manuscript and conducted the cell viability assay. DXZ, WC and HL performed the other activity tests. XYL and YXL were involved in the analysis and interpretation of the data.

DW contributed to the conception and design of the study, critically revised the manuscript and provided final approval of the version to be published. All the authors have read and approved the final version of the manuscript.

Ethics approval and consent to participate

The study protocol complied with the recommendations of the Guide for the Care and Use of Laboratory Animals of the Shenyang Pharmaceutical University and all animal experiments were approved by the Committee on the Ethics of Animal Experiments of the Shenyang Pharmaceutical University.

Patient consent for publication

Not applicable.

Competing interests

All the authors declare that they have no competing interests.

References

1. Herbst RS, Morgensztern D and Boshoff C: The biology and management of non-small cell lung cancer. Nature 553: 446-454, 2018.
2. Chen Z, Fillmore CM, Hammerman PS, Kim CF and Wong KK: Non-small-cell lung cancers: A heterogeneous set of diseases. Nat Rev Cancer 14: 535-546, 2014.
3. Zhang C, Leighl NB, Wu YL and Zhong WZ: Emerging therapies for non-small cell lung cancer. J Hematol Oncol 12: 45, 2019.
4. Terlizzi M, Colarusso C, Pinto A and Sorrentino R: Drug resistance in non-small cell lung cancer (NSCLC): Impact of genetic and non-genetic alterations on therapeutic regimen and responsiveness. Pharmacol Ther 202: 140-148, 2019.
5. Shih JC, Chen K and Ridd MJ: Monoamine oxidase: From genes to behavior. Annu Rev Neurosci 22: 197-217, 1999.
6. Brunner HG, Nelen M, Breakefield XO, Ropers HH and Van Oost BA: Abnormal behavior associated with a point mutation in the structural gene for monoamine oxidase A. Science 262: 578-580, 1993.
7. Schwartz TL: A neuroscientific update on monoamine oxidase and its inhibitor. CNS Spectr 18 (Suppl 1): S25-S33, 2013.
8. Lin YC, Chang YT, Campbell M, Lin TP, Pan CC, Lee HC, Shih JC and Chang PC: MAOA-a novel decision maker of apoptosis and autophagy in hormone refractory neuroendocrine prostate cancer cells. Sci Rep 7: 46338, 2017.
9. Wu JB, Shao C, Li X, Li Q, Hu P, Shi C, Li Y, Chen YT, Yin F, Liao CP, *et al*: Monoamine oxidase A mediates prostate tumorigenesis and cancer metastasis. J Clin Invest 124: 2891-2908, 2014.
10. Li PC, Siddiqi IN, Mottok A, Loo EY, Wu CH, Cozen W, Steidl C and Shih JC: Monoamine oxidase A is highly expressed in classical Hodgkin lymphoma. J Pathol 243: 220-229, 2017.
11. Shih JC: Monoamine oxidase isoenzymes: Genes, functions and targets for behavior and cancer therapy. J Neural Transm (Vienna) 125: 1553-1566, 2018.
12. Kushal S, Wang W, Vaikari VP, Kota R, Chen K, Yeh TS, Jhaveri N, Groshen SL, Olenyuk BZ, Chen TC, *et al*: Monoamine oxidase A (MAO A) inhibitors decrease glioma progression. Oncotarget 7: 13842-13853, 2016.
13. Wu JB, Lin TP, Gallagher JD, Kushal S, Chung LW, Zhau HE, Olenyuk BZ and Shih JC: Monoamine oxidase A inhibitor-near-infrared dye conjugate reduces prostate tumor growth. J Am Chem Soc 137: 2366-2374, 2015.
14. Liu F, Hu L, Ma Y, Huang B, Xiu Z, Zhang P, Zhou K and Tang X: Increased expression of monoamine oxidase A is associated with epithelial to mesenchymal transition and clinicopathological features in non-small cell lung cancer. Oncol Lett 15: 3245-3251, 2018.
15. Yang X, Shao C, Wang R, Chu CY, Hu P, Master V, Osunkoya AO, Kim HL, Zhai HE and Chung LWK: Optical imaging of kidney cancer with novel near infrared heptamethine carbocyanine fluorescent dyes. J Urol 189: 702-710, 2013.
16. Yang X, Shi C, Tong R, Qian W, Zhau HE, Wang R, Zhu G, Cheng J, Yang VW, Cheng T, *et al*: Near IR heptamethine cyanine dye-mediated cancer imaging. Clin Cancer Res 16: 2833-2844, 2010.
17. Yi X, Yan F, Wang F, Qin W, Wu G, Yang X, Shao C, Chung LW and Yuan J: IR-780 dye for near-infrared fluorescence imaging in prostate cancer. Med Sci Monit 21: 511-517, 2015.
18. Wang Y, Liu T, Zhang E, Luo S, Tan X and Shi C: Preferential accumulation of the near infrared heptamethine dye IR-780 in the mitochondria of drug-resistant lung cancer cells. Biomaterials 35: 4116-4124, 2014.
19. Huang H, Long S, Li M, Gao F, Du J, Fan J and Peng X: Bromo-pentamethine as mitochondria-targeted photosensitizers for cancer cell apoptosis with high efficiency. Dyes Pigments 149: 633-638, 2018.
20. Shi C, Wu JB and Pan D: Review on near-infrared heptamethine cyanine dyes as theranostic agents for tumor imaging, targeting, and photodynamic therapy. J Biomed Opt 21: 50901, 2016.
21. Zhang E, Luo S, Tan X and Shi C: Mechanistic study of IR-780 dye as a potential tumor targeting and drug delivery agent. Biomaterials 35: 771-778, 2014.
22. Usama SM, Lin CM and Burgess K: On the mechanisms of uptake of tumor-seeking cyanine dyes. Bioconjug Chem 29: 3886-3895, 2018.
23. Yang XG, Mou YH, Wang YJ, Wang J, Li YY, Kong RH, Ding M, Wang D and Guo C: Design, synthesis, and evaluation of monoamine oxidase A inhibitors-indocyanine dyes conjugates as targeted antitumor agents. Molecules 24: 1400, 2019.
24. Wu JB, Chen K, Li Y, Lau YF and Shih JC: Regulation of monoamine oxidase A by the SRY gene on the Y chromosome. FASEB J 23: 4029-4038, 2009.
25. Wang L, Chen G, Lu X, Wang S, Han S, Li Y, Ping G, Jiang X, Li H, Yang J and Wu C: Novel chalcone derivatives as hypoxia-inducible factor (HIF)-1 inhibitor: Synthesis, anti-invasive and anti-angiogenic properties. Eur J Med Chem 89: 88-97, 2015.
26. Wang LH, Jiang XR, Yang JY, Bao XF, Chen JL, Liu X, Chen GL and Wu CF: SYP-5, a novel HIF-1 inhibitor, suppresses tumor cells invasion and angiogenesis. Eur J Pharmacol 791: 560-568, 2016.
27. Valastyan S and Weinberg RA: Tumor metastasis: Molecular insights and evolving paradigms. Cell 147: 275-292, 2011.
28. Kai F, Drain AP and Weaver VM: The extracellular matrix modulates the metastatic journey. Dev Cell 49: 332-346, 2019.
29. Brown Y, Hua S and Tanwar PS: Extracellular matrix-mediated regulation of cancer stem cells and chemoresistance. Int J Biochem Cell Biol 109: 90-104, 2019.
30. Eble JA and Niland S: The extracellular matrix in tumor progression and metastasis. Clin Exp Metastasis 36: 171-198, 2019.
31. Kleiner DE and Stetler-Stevenson WG: Matrix metalloproteinases and metastasis. Cancer Chemother Pharmacol 43 (Suppl): S42-S51, 1999.
32. Chiu KH, Chang YH, Wu YS, Lee SH and Liao PC: Quantitative secretome analysis reveals that COL6A1 is a metastasis-associated protein using stacking gel-aided purification combined with iTRAQ labeling. J Proteome Res 10: 1110-1125, 2011.
33. Hou T, Tong C, Kazobinka G, Zhang W, Huang X, Huang Y and Zhang Y: Expression of COL6A1 predicts prognosis in cervical cancer patients. Am J Transl Res 8: 2838-2844, 2016.
34. Theocharis AD, Skandalis SS, Gialeli C and Karamanos NK: Extracellular matrix structure. Adv Drug Deliv Rev 97: 4-27, 2016.
35. Semenza GL: Hypoxia-inducible factors: Mediators of cancer progression and targets for cancer therapy. Trends Pharmacol Sci 33: 207-214, 2012.
36. Gonzalez-Avila G, Sommer B, Mendoza-Posada DA, Ramos C, Garcia-Hernandez AA and Falfan-Valencia R: Matrix metalloproteinases participation in the metastatic process and their diagnostic and therapeutic applications in cancer. Crit Rev Oncol Hematol 137: 57-83, 2019.
37. Hafner C, Landthaler M and Vogt T: Activation of the PI3K/AKT signalling pathway in non-melanoma skin cancer is not mediated by oncogenic PIK3CA and AKT1 hotspot mutations. Exp Dermatol 19: e222-e227, 2010.
38. Nödling AR, Mills EM, Li X, Cardella D, Sayers EJ, Wu SH, Jones AT, Luk LYP and Tsai YH: Cyanine dye mediated mitochondrial targeting enhances the anti-cancer activity of small-molecule cargoes. Chem Commun (Camb) 56: 4672-4675, 2020.
39. Choi PJ, Park TIH, Cooper E, Dragunow M, Denny WA and Jose J: Heptamethine cyanine dye mediated drug delivery: Hype or hope. Bioconjug Chem 31: 1724-1739, 2020.